Supporting Information

High-Performance Inkjet-Printed Indium-Gallium-Zinc-Oxide Transistors Enabled by Embedded, Chemically Stable Graphene Electrodes

Ethan B. Secor[†], Jeremy Smith[‡,∥], Tobin J. Marks[†,‡,], and Mark C. Hersam[†,‡,§,*]*

† Department of Materials Science and Engineering and the Materials Research Center, Northwestern University, Evanston, IL 60208, USA

‡ Department of Chemistry and the Materials Research Center, Northwestern University, Evanston, IL 60208, USA

§ Department of Electrical Engineering and Computer Science, Northwestern University, Evanston, IL 60208, USA

* Corresponding authors: t-marks@northwestern.edu; m-hersam@northwestern.edu

1. Device Fabrication Details

Silver/IGZO. For fabrication of IGZO TFTs with silver contacts, five layers of IGZO ink were printed onto Si/SiO_2, with annealing at 300 °C for 15 min after each layer. After the fifth layer, the IGZO film was annealed at 300 °C for 45 min in a humidity-controlled environment (RH < 5%). Immediately after annealing, silver electrodes were inkjet printed and annealed at 200 °C for 5 min.

Top-contact graphene/IGZO. For fabrication of IGZO TFTs with graphene electrodes in a top-contact structure, five layers of IGZO ink were printed onto Si/SiO_2, with annealing at 300 °C for 15 min after each layer. Graphene electrodes were then inkjet printed, followed by annealing at 300 °C for 20 min. Finally, the TFTs were annealed at 300 °C for 45 min in a humidity-controlled environment (RH < 5%).

Bottom-contact graphene/IGZO. For fabrication of IGZO TFTs with graphene electrodes in a bottom-contact structure, graphene electrodes were printed onto Si/SiO_2 and annealed at 300 °C for 20 min. Following air plasma treatment of the substrate with printed graphene electrodes (Harrick Plasma PDC-32G, low power, 2 min, 200 mTorr), five layers of IGZO ink were printed, with annealing at 300 °C for 15 min after each layer. Following the deposition of all materials, the TFTs were annealed at 300 °C for 45 min in a humidity-controlled environment (RH < 5%).

Middle-contact graphene/IGZO. For fabrication of IGZO TFTs with graphene electrodes in a middle-contact structure, three layers of IGZO ink were printed onto a plasma-treated (high power, 5 min, 300 mTorr) Si/SiO_2 substrate, with annealing at 300 °C for 15 min after each layer. Graphene electrodes were then inkjet printed and annealed at 300 °C for 20 min. A second air plasma treatment step was performed (low power, 2 min, 200 mTorr) to ensure good wetting on the graphene patterns, after which two additional layers of IGZO ink were printed, with annealing at 300 °C for 15 min after each layer. Following the deposition of all materials, the TFTs were annealed at 300 °C for 45 min in a humidity-controlled environment (RH < 5%). The configuration for all reported data of MC TFTs is as described here, namely 3 IGZO printing passes, then graphene electrodes, followed by 2 additional IGZO printing passes. While other configurations were tested for optimization, no clear difference was observed for 2-4 initial IGZO printing passes.

2. Silver/IGZO TFT Characterization (Figure S1)

As shown in Figure 1, the electrical performance of IGZO TFTs with silver electrodes is poor and unstable. To provide insight into the underlying chemistry and physics, and to verify that more optimal processing conditions will not mitigate these issues, silver/IGZO TFTs were fabricated with varying annealing temperatures for the silver electrodes. The silver nanoparticle ink requires annealing at 150 °C for highly conductive films, so this was selected as the minimum temperature condition. As shown in Figure S1, devices annealed at 150 °C exhibit poor electron mobility of < 0.1 $cm^2/V{\cdot}s$. As the annealing temperature is increased, the performance improves slightly to a peak mobility of ~0.3 $cm^2/V{\cdot}s$ for 200 °C processing, although the device-to-device variation remains high. At higher temperatures, the performance again decreases, likely due to silver migration and oxide formation at the contact interface. Although silver could conceivable migrate into the oxide gate dielectric as well, with a relatively thick (300 nm) dielectric, we do not observe increased gate leakage (Figure S1c).

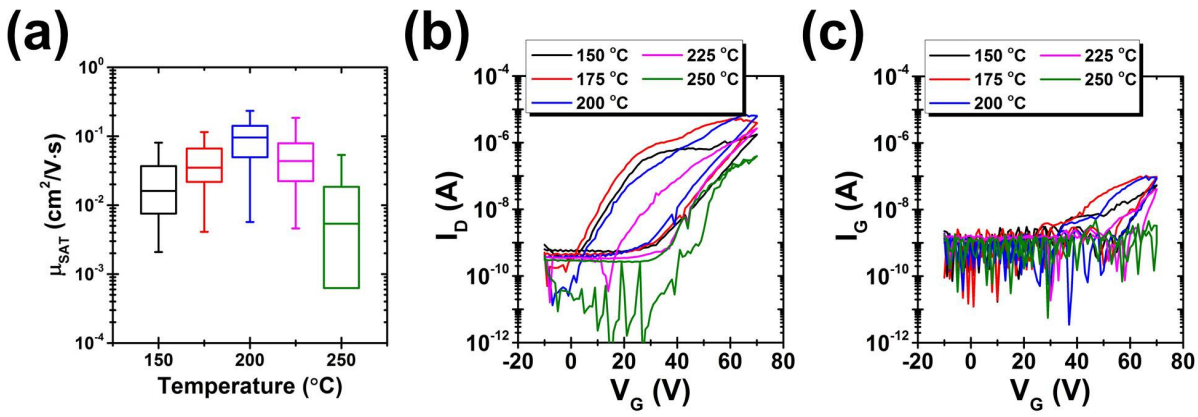

Figure S1. Annealing optimization for IGZO TFTs with silver contacts. (a) Box plots of mobility for IGZO with silver contacts fabricated with processing temperatures from 150-250 °C (n = 31, 5 min annealing in ambient at the specified temperature in each case). (b,c) Representative transfer curves and corresponding gate leakage, respectively, for IGZO TFTs with silver contacts.

3. Output characteristics for non-optimal device structures (Figure S2)

As discussed in the main narrative, IGZO TFTs with silver contacts exhibit unstable and poor electrical performance. A representative output curve for a silver/IGZO TFT with the optimal annealing temperature of 200 °C is shown in Figure S2a. The nonlinearity at low drain bias is indicative of an injection barrier, and the decrease in current at high drain bias suggests

the prevalence of charge traps. For IGZO TFTs with graphene contacts, both BC and TC devices also have limitations. Figure 2 displays output characteristics for these devices. In addition, full-scale output characteristics for BC and TC devices are shown in Figure S2b-c.

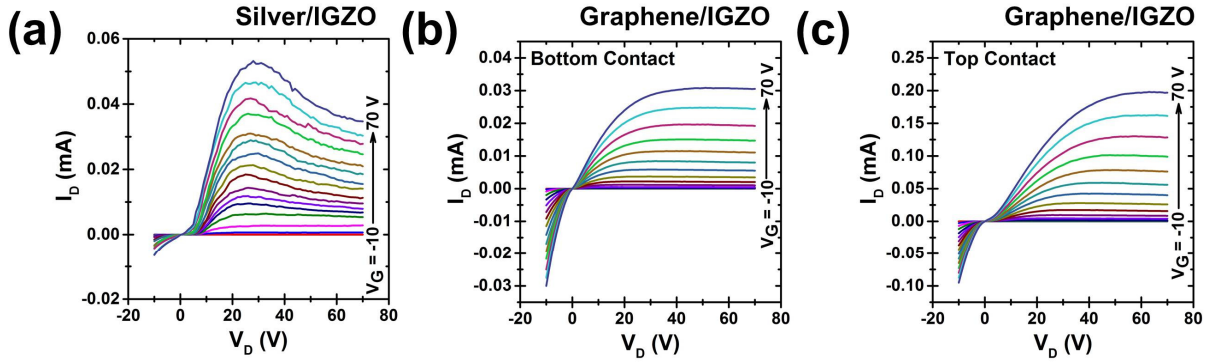

Figure S2. Representative output curves for non-optimal IGZO devices. (a) Output characteristics for an IGZO TFT with silver source/drain contacts, following optimal annealing at 200 °C. (b,c) Output characteristics for IGZO TFTs with graphene bottom and top contacts, respectively. Note the low drain current for the case of (b), and the nonlinearity at low bias for (c).

4. Device characterization (Figure S3, S4)

Morphological characterization is carried out to examine the physical features of inkjet-printed devices. Figure S3 shows AFM images of a bottom-contact graphene-IGZO device near the channel boundary (a) and toward the center of the electrode (b). These images confirm that the amorphous IGZO forms a dense and uniform film when deposited directly on SiO_2, with a RMS roughness of ~0.29 nm. In contrast, the roughness of the graphene electrode is measured to be ~28 nm. This difference in surface morphology is a key distinguishing characteristic between the device geometries, and likely leads to higher mobility in TC and MC TFTs.

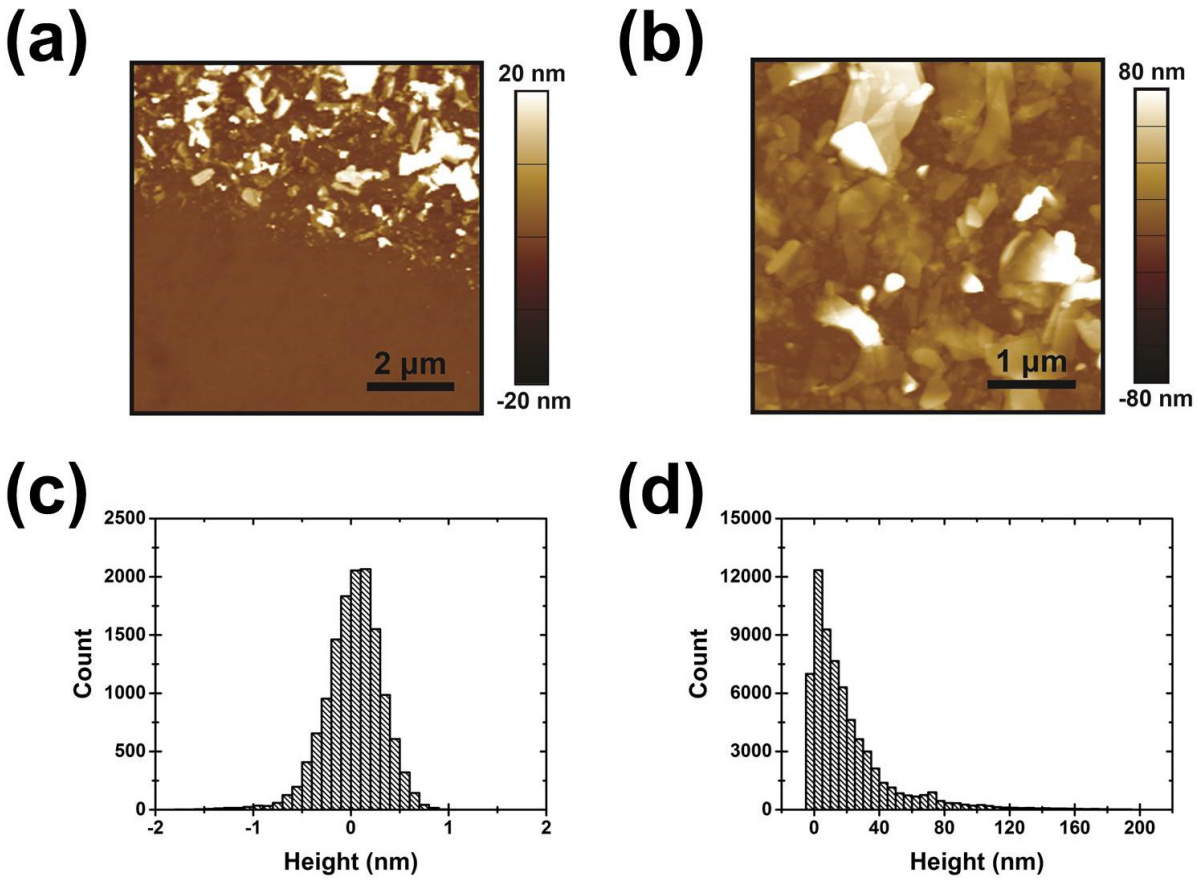

Figure S3. Atomic force microscopy characterization of an IGZO TFT with graphene contacts. (a,b) AFM topography images at the channel-electrode interface and at the center of the electrode, respectively. (c,d) Height histograms for regions on the IGZO film and on the graphene electrode, respectively.

Larger-area characterization is provided in Figure S4, which shows a typical optical microscopy image and a profilometry scan across the IGZO film. These results indicate a thickness of ~15 nm, or 3 nm/pass. As such, the roughness of a graphene bottom electrode is high relative to the total thickness of the deposited IGZO film.

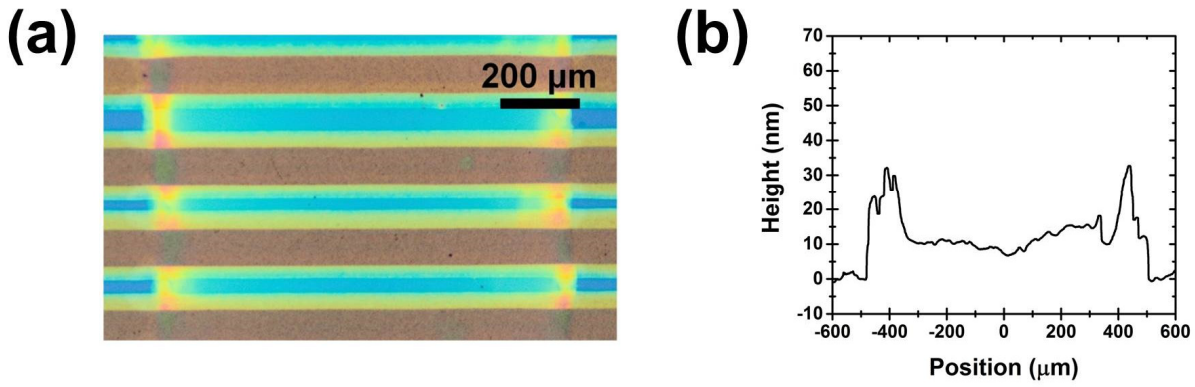

Figure S4. (a) Optical microscopy image of IGZO TFTs with graphene contacts inkjet-printed on Si/SiO_2. (b) Thickness profile across an inkjet-printed IGZO film following five printing passes, showing an average thickness of 15 nm.

5. Statistics for different device structures (Figure S5, S6, S7)

Figure 3a displays the saturation mobility for MC devices with varying channel lengths. Figure S5 shows corresponding data for TC and BC devices, along with the MC devices. The fairly linear increase in mobility with channel length for BC devices suggests that these devices are contact-limited. It is evident that MC devices display the best performance. Additional transistor metrics, including the current on/off ratio and threshold voltage, are shown for MC devices in Figure S6. The reduction in mobility for devices with short channel length can be related to contact resistance effects. For a simple comparison of the different device geometries, we take the ratio of mobility for devices with channel length of 600 µm and 75 µm. A larger ratio indicates a more significant effect of the contacts. The resulting ratios are 2.21, 1.44, and 1.44 for devices with BC, TC, and MC geometries, respectively. To investigate this in more detail, we extract contact resistance for the different device geometries.

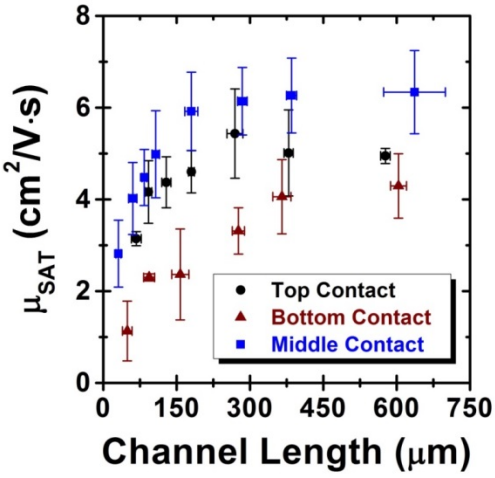

Figure S5. Measured mobility for top, bottom, and middle contact devices as a function of channel length (n = 40, 25, 122 for TC, BC, and MC, respectively).

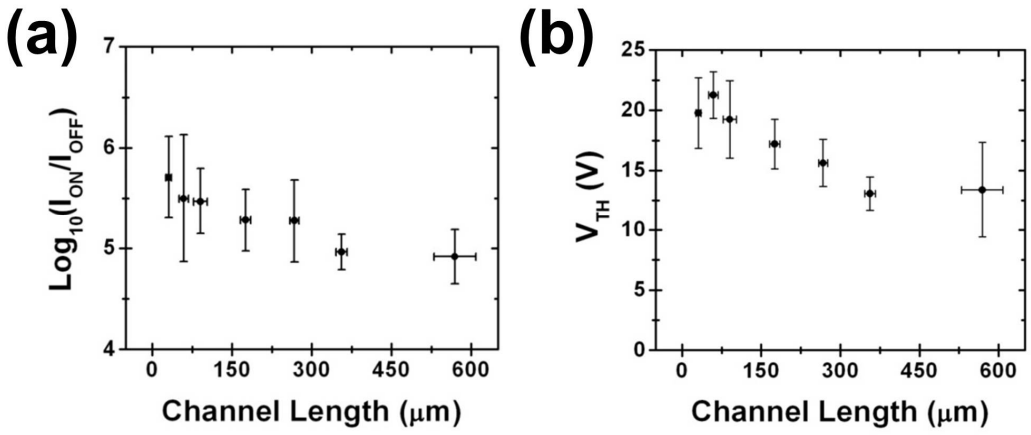

Figure S6. Electrical characteristics of MC IGZO TFTs with graphene contacts. (a,b) Current on/off ratio (I_{ON}/I_{OFF}) and threshold voltage (V_{TH}), respectively, plotted against channel length (n = 122).

Figures 3b and 3c display the contact resistance extraction for MC devices. Figure S7 shows corresponding data for TC and BC devices. Although the TC devices show a similar contact resistance to MC devices, it is important to note that these devices exhibit nonlinearity in the output curves. To calculate total resistance in this case, the lowest-resistance region of the output curves are used. The BC TFTs exhibit a higher contact resistance, consistent with the slow increase in calculated mobility with increasing channel length (Figure S5). The contact resistance of these devices is one contribution to the decreased mobility measured for TFTs with shorter channel lengths.

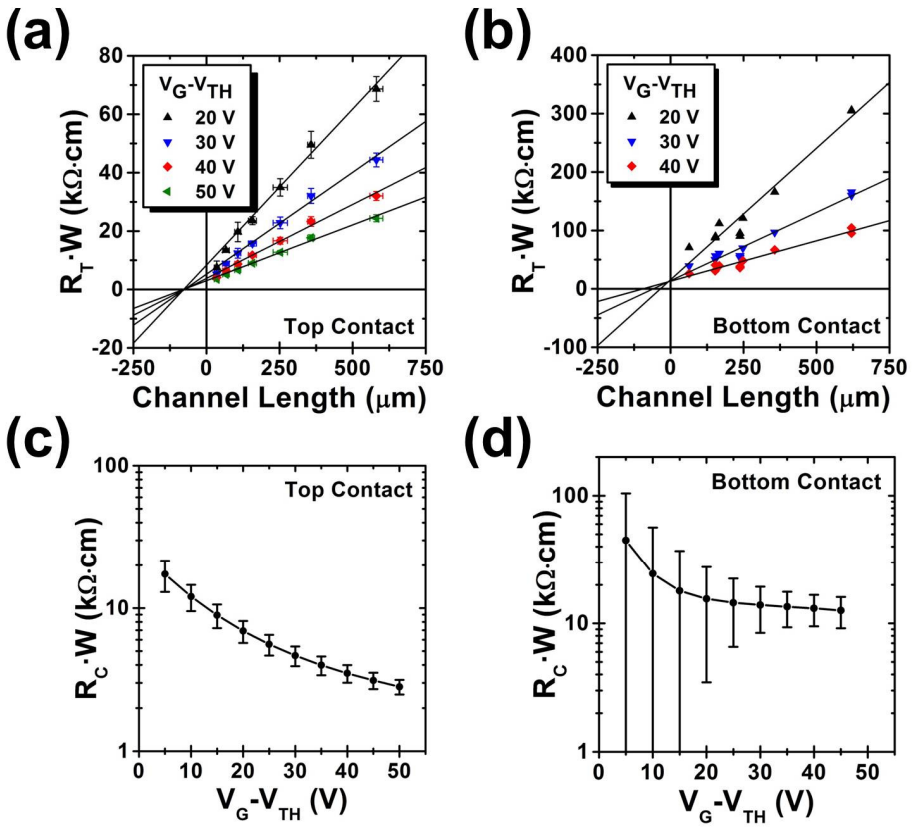

Figure S7. Contact resistance measurements for IGZO TFTs with graphene contacts. (a,b) Total resistance plotted against channel length for top contact and bottom contact devices, respectively. (c,d) Contact resistance plotted against gate bias for top contact and bottom contact devices, respectively.

With the contact resistance measurements for IGZO TFTs with different contact geometries, it is possible to calculate mobility corrected for the contact resistance. The measured total resistance is used to calculate channel resistance using the relation

$$R_T = \frac{\partial V_{DS}}{\partial I_{DS}} = r_{ch}L + R_C \quad (1)$$

in which R_T is the total resistance, R_C is the contact resistance, and $r_{ch}L$ denotes the channel resistance. The corrected mobility is calculated as

$$\mu_{corr} = \frac{1}{C_i W} \frac{\partial(\frac{1}{r_{ch}})}{\partial V_G} \quad (2)$$

in which C_i is the gate capacitance, W is the channel width, and V_G is the gate voltage. This analysis was applied to IGZO TFTs with the three different contact geometries, and the corrected

mobility for BC, TC, and MC devices was calculated to be 3.51 ± 1.29, 5.68 ± 0.89, and 9.61 ± 1.27 $cm^2/V{\cdot}s$, respectively.

6. Hysteresis of IGZO TFTs (Figure S8)

As shown in Figure 1c, modest hysteretic behavior is evident in the transfer characteristics of the IGZO TFTs with graphene contacts. While this is small relative to that observed for IGZO TFTs with silver contacts, it affects the electrical measurements of devices. We note that all reported data is obtained using the forward sweep of the transfer curve. In Figure S8, we provide more thorough details of the hysteretic behavior for the MC IGZO devices reported in the manuscript (number of devices, n = 122). Figure S8a shows the threshold voltage hysteresis calculated from the forward and reverse sweeps of the transfer curve, indicating greater hysteresis for shorter channel length devices. Figure S8b shows the corresponding data for the calculated mobility, indicating similar channel length dependence and a higher mobility calculated from the reverse sweep. Figure S8c shows the average calculated mobility from the transconductance of the forward and reverse voltage sweeps as a function of channel length. Compared to Figure 3a, the channel length dependence is greatly reduced when the forward and reverse sweeps are averaged. While this does not represent a true mobility, it suggests that hysteretic effects are one source of the decrease in mobility for TFTs with shorter channel lengths.

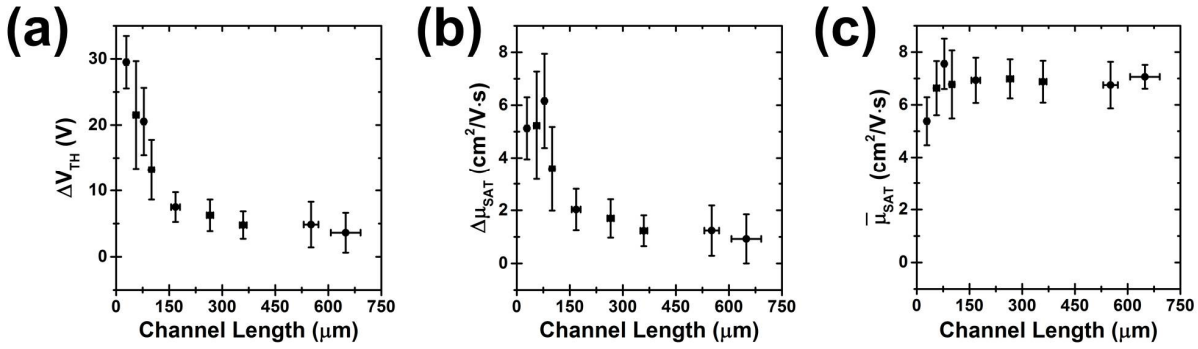

Figure S8. Characterization of hysteresis for MC IGZO TFTs with graphene contacts. (a) Threshold voltage hysteresis from the forward and reverse sweeps of the transfer characteristics. (b) Difference in calculated mobility based on the forward and reverse voltage sweeps. (c) Calculated mobility plotted

against channel length using the average mobility calculated from the forward and reverse voltage sweeps. Number of devices, n = 122.

7. Aging stability of IGZO TFTs with graphene electrodes (Figure S9)

The stability of IGZO TFTs upon aging in ambient is discussed in the main narrative. Additional information is provided in Figure S9, including transfer curves for a single device and statistics for the threshold voltage. While the threshold voltage shows an initial shift, it remains at a low, positive value for the remaining time, with small fluctuations likely due to environmental factors such as humidity and no systematic shifts.

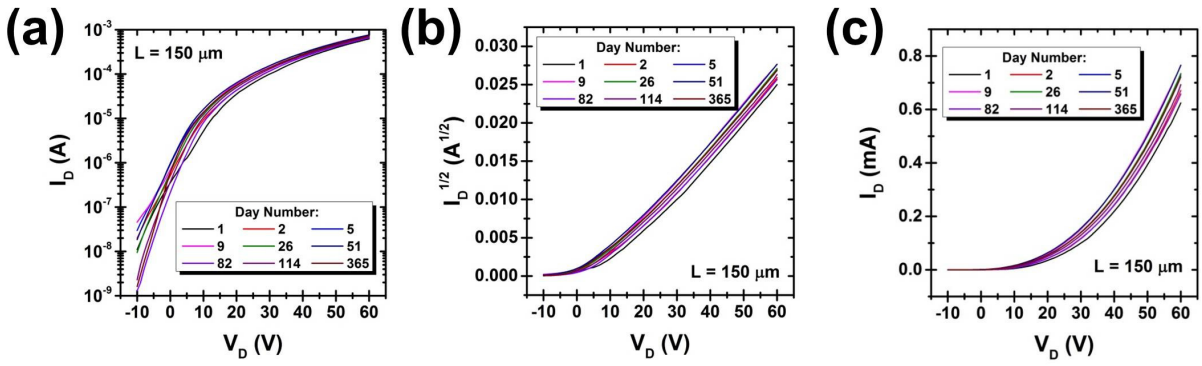

Figure S9. Electrical performance of MC graphene/IGZO TFTs during aging in ambient conditions. (a-c) Transfer characteristics for a single device measured nine times over the course of 365 days, with different axes scaling.

8. Integration of graphene/IGZO TFTs with silver interconnects (Figure S10)

Although graphene presents a superior contact material to IGZO compared to silver, silver remains a desirable material to use for printed interconnects and wires due to its excellent electrical conductivity. Therefore, a suitable device format would include IGZO TFTs with graphene contacts connected to the larger circuit with silver interconnects. To confirm that the graphene presents a stable interface with silver, as well as a suitable barrier between silver and IGZO, TFTs were fabricated using contacts composed of both silver and graphene concurrently. As shown in Figure S10, a layer of silver was inserted into standard MC graphene/IGZO TFTs. Because the contact-channel interface is at the leading edge of the graphene contact, which is not covered with silver, a second layer of graphene on top of the silver was unnecessary. An optical

micrograph of the devices is shown in Figure S10b. The devices exhibit performance metrics nominally identical to MC devices without silver (Figure S10c), confirming that this strategy is suitable for integrating these IGZO TFTs into larger circuits using silver interconnects.

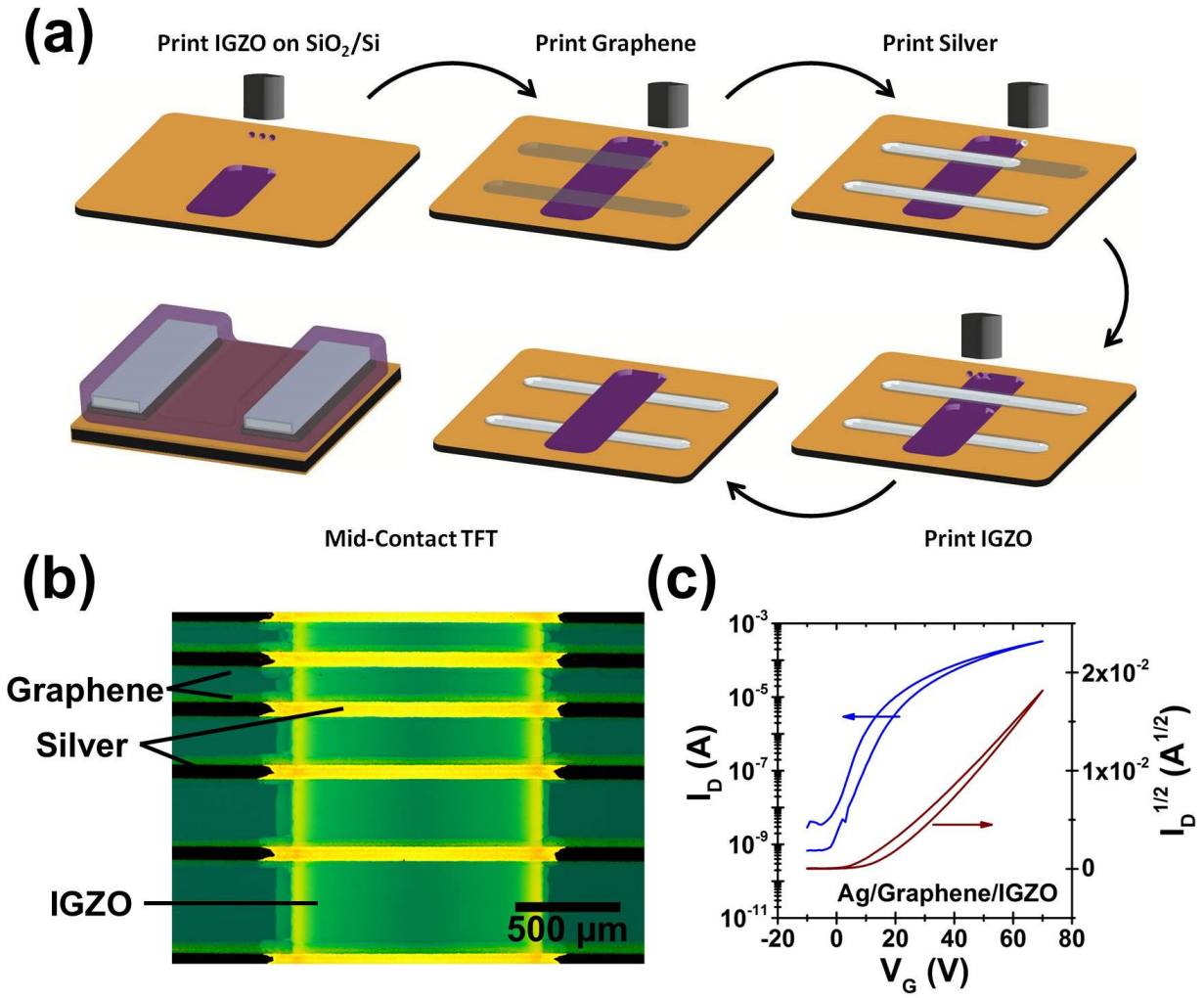

Figure S10. Connection of graphene/IGZO TFTs with silver interconnects. (a) Schematic illustration showing TFT fabrication process with silver inserted into standard MC graphene/IGZO TFTs. (b) Optical micrograph showing the printed devices, with the different materials indicated. (c) Representative transfer curve for the TFTs.